

Prepared in cooperation with the U.S. Geological Survey Water Availability and Use Science Program

MODFLOW 6 CSUB Package Example Problems

Version mf6.1.0—December 13, 2019

U.S. Department of the Interior
U.S. Geological Survey

Cover. Binary computer code illustration.

Contents

Introduction	1
Example Problems	1
Problem 1 – Elastic aquifer loading	1
Problem 2 – Delay interbed drainage	5
Problem 3 – One-dimensional compaction	10
Problem 4 – One-dimensional compaction in a three-dimensional flow field	18
References Cited	R-1

Figures

1. Diagram showing the model domain for the elastic aquifer loading problem	1
2. Graphs showing the applied loading and water-level fluctuations for the elastic aquifer loading problem	3
3. Diagram showing the model domain and setup for the delay interbed drainage problem	6
4. Graphs showing comparisons of simulated compaction with the head-based formulation and the analytical solution for the delay interbed drainage problem	7
5. Graphs showing comparisons of simulated compaction for head- and effective stress-based formulations for the delay interbed drainage problem	8
6. Graphs showing differences between head- and effective stress-based compaction for different interbed thicknesses for the delay interbed drainage problem	9
7. Graphs showing differences between head- and effective stress-based formulation interbed heads relative to head-based interbed heads for variable interbed thicknesses at select fractions of the time constant for the delay interbed drainage problem	9
8. Maps showing the location of the study area for the one-dimensional compaction problem in southern California	10
9. Diagram showing the model domain and setup for the one-dimensional compaction problem	11
10. Graph showing depth to water values used in the one-dimensional compaction problem for the upper, middle, and lower aquifers at the Holly site, Edwards Air Force Base, Antelope Valley, California. Modified from Snead (2008)	13
11. Graphs showing simulated compaction in different material types using head- and effective stress based formulations for the one-dimensional compaction problem	14
12. Graphs showing history matches for simulated and observed aquifer-system compaction in the one-dimensional compaction problem	16
13. Graph showing simulated vertical head profiles and approximately decadal head changes in the one-dimensional compaction problem	17
14. Diagram showing the model domain for the one-dimensional compaction in a three-dimensional flow field problem	18

15. Graphs showing computed stresses for row 9, column 10 for the one-dimensional compaction in a three-dimensional flow field problem	21
16. Graphs showing computed downward displacement for the tops of model layers 1–4 for the one-dimensional compaction in a three-dimensional flow field problem	22

Tables

1. Assumed train length and weight for the elastic aquifer loading problem	2
2. Hydraulic properties for the elastic aquifer loading problem	2
3. Aquifer system thickness and hydraulic properties for the one-dimensional compaction problem	12
4. Coarse-grained material thickness and hydraulic properties for the one-dimensional compaction problem	15
5. Fine-grained material no-delay and delay interbed thickness and hydraulic properties for the one-dimensional compaction problem. Equivalent interbed thickness and delay interbed material factor values are defined for delay interbeds.	15
6. Coarse-grained material hydraulic properties for the one-dimensional compaction in a three-dimensional flow field problem	19
7. Fine-grained material hydraulic properties for the one-dimensional compaction in a three-dimensional flow field problem	19
8. Specific gravity of saturated and moist materials for the one-dimensional compaction in a three-dimensional flow field problem	20

Introduction

This document describes example problems for the Groundwater Flow (GWF) model skeletal storage, compaction and subsidence (CSUB) Package of MODFLOW 6. The examples demonstrate use of the capabilities of the CSUB package including: 1) elastic compaction of coarse grained aquifer materials, 2) inelastic and elastic compaction of thin interbeds of fine-grained materials that equilibrate quickly with head changes in coarse grained aquifer materials, and 3) inelastic and elastic compaction of thick interbeds of fine-grained materials that require time to equilibrate with head changes in coarse grained aquifer materials. This document also details differences between models that use the effective stress and head-based formulations to simulate compaction and some typical analyses that can be completed using the CSUB package output.

Example Problems

Problem 1 – Elastic aquifer loading

This problem simulates elastic compaction of aquifer materials in response to the loading of an aquifer by a passing train. Water-level responses were simulated for an eastbound train leaving the Smithtown Station in Long Island, New York at 13:04 on April 23, 1937 ([Jacob, 1939](#)).

The problem is simulated as a two-dimensional half-cell cross-section model. The model grid for this problem consists of three layers, 1 row, and 35 columns (fig. 1). The model layers were defined based on hydrostratigraphic information in [Jacob \(1939\)](#). The upper and lower layer represent an unconfined upper aquifer and confined lower aquifer separated by a confining unit (fig. 1B). The upper and lower aquifers are composed of sand and gravel, respectively, and the confining unit is composed of clay.

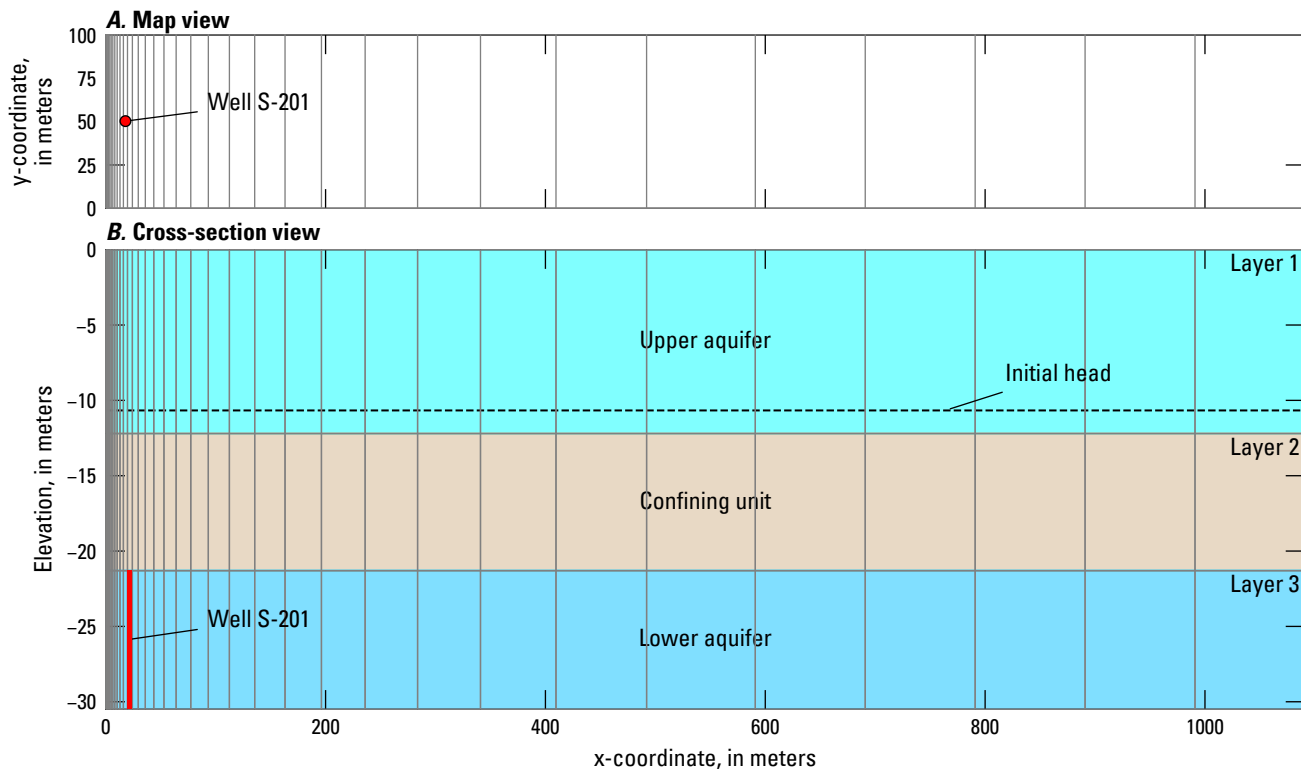


Figure 1. Diagram showing the model domain for the elastic aquifer loading problem. *A*, plan view, and *B*, cross-section view.

2 MODFLOW 6 CSUB Package Example Problems

The model has a top elevation of 0 meters and layer bottom elevations of -12.2, -21.3, and -30.5 meters, for layers 1, 2, and 3 respectively. DELR increases from 0.5 to 98.9 meters in columns 1 to 30, using a multiplier of 1.2; a DELR value of 100 meters is specified in columns 31 to 35. DELC is specified with a constant value of 100.6 meters and is based on the an estimate of the total length of the train (table 1). The simulation consists of two stress periods. The first stress period is steady-state with a single time step and is 0.5 seconds in length. The second stress period is transient, 58.5 seconds in length, and is divided into 117 equally sized time steps.

Table 1. Assumed train length and weight for the elastic aquifer loading problem.

Type	Number	Length, in meters	Weight, in kilograms
Engine	2	21.3	108,862.08
Car	4	79.3	199,580.48
Total	—	100.6	308,442.56

Initial hydraulic properties were based on aquifer material data in [Freeze and Cherry \(1979\)](#) and are summarized in table 2. Hydraulic conductivity was assumed to be isotropic in the horizontal and vertical directions in each layer. Hydraulic conductivity and specific storage values were modified from initial values during model calibration, which is described below. The specific storage was defined to be 0 for all layers in the storage (STO) package. All model layers were defined to be convertible for hydraulic conductivity and storage properties. Default flow property (NPF) and storage (STO) package settings were used. An initial head of -10.7 meters was defined for each layer.

Table 2. Hydraulic properties for the elastic aquifer loading problem.

Layer	Hydraulic conductivity, in meters per second	Total porosity, unitless	Specific yield, unitless	Specific storage, in per meter
1	1.8×10^{-5}	0.25	0.10	3.3×10^{-5}
2	3.5×10^{-10}	0.50	0.05	6.6×10^{-7}
3	3.1×10^{-5} †	0.30	0.30	4.5×10^{-7} †

† calibrated

The effective stress formulation of the CSUB package was used to simulate one-dimensional compaction of aquifer materials. A specific gravity of 1.7 and 2.0 was defined for moist and saturated sediments, respectively. Water compressibility was simulated using a specific gravity of water of 9,806.65 Newtons per cubic meters and water compressibility of 4.6512×10^{-10} per Pascal. The thickness of compressible materials and total porosity were updated during the simulation in response compaction.

[Jacob \(1939\)](#) measured water-level fluctuations in well S-201 (fig. 1A). S-201 is located 16.5 meters north of the tracks (column 12) and has a total depth of 27.1 meters (model layer 3). A limited amount of data on the position of the train relative to well S-201 was provided by [Jacob \(1939\)](#). As a result, it was assumed that the original water-level fluctuation data is a proxy for train loading. The maximum water-level fluctuation value was assumed to correspond to loading by the full weight of the train (table 1) and a zero water-level fluctuation corresponded to complete unloading. The estimated loading of the aquifer (fig. 2A) was converted to an equivalent height of water over the first cell of the model using the cell area, one-half the total train weight (because

the problem is simulated as a half-cell problem), and the density of water (1,000 kilograms per cubic meters). Because well S-201 is located 16.5 meters north of the tracks, the estimated loading was translated in time by -1.5 seconds to account for the time for loading to cause water-level fluctuations at the well; the -1.5 second adjustment was determined through trial and error. Train loading was applied in column 1 using a time series file. Flow was not allowed to leave the model domain and no sources/sinks were applied to the model. The left and right side of the model domain are represented as a free-slip (roller) boundaries.

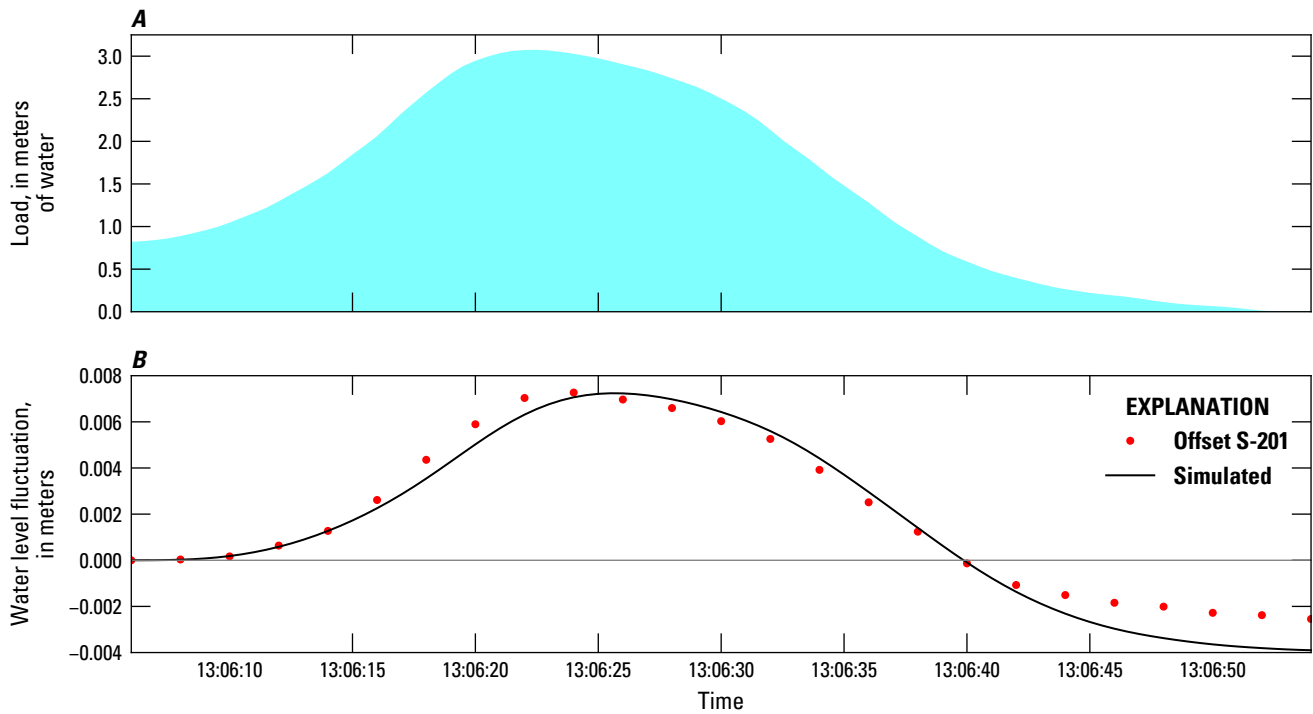


Figure 2. Graphs showing the applied loading and water-level fluctuations for the elastic aquifer loading problem. *A*, shows the loading applied to the top of the first column in layer 1, and *B*, shows simulated and offset water-level fluctuations at well S-201.

The water-level fluctuation data used to calibrate the hydraulic parameters was offset so that the initial water-level fluctuation reported (after rewinding the pen-carriage cable) corresponded to a zero value. The adjusted water-level at the end of the simulation period is less than zero since loading of the aquifer by the train was already occurring at the beginning of the data presented in Jacob (1939) (fig 2*B*). The water-level fluctuation data was offset rather than extended because of uncertainties about the train velocity and acceleration prior to the simulation period.

PEST++ (Welter and others, 2015) was used to calibrate the horizontal hydraulic conductivity in layers 1 and 3, the vertical hydraulic conductivity in layer 2, and specific storage values in all model layers. The water-level fluctuation observations were weighted by $\max(0.01, h_i/\max(h))$ to force PEST++ to favor the peak water-level fluctuations. The water-level fluctuations were only sensitive to the hydraulic conductivity and specific storage of model layer 3; as a result, PEST++ only modified the hydraulic properties of layer 3. Final hydraulic properties used in the model are shown in table 2.

A comparison of simulated and observed water-level fluctuations is shown in figure 2*B*. For this problem, the MODFLOW 6 solution does not show perfect agreement with the offset water-level fluctuations. The primary source of model error is likely due primarily to inaccuracies in the loading being applied in the model. Use of a two-dimensional cross-section model instead of a three-dimensional model may also be responsi-

4 MODFLOW 6 CSUB Package Example Problems

ble for a portion of the model error shown in figure 2B. Horizontal strain has also been found to be significant in close proximity pumping wells (the source of strain) and may also contribute to the model error ([Burbey, 2001](#)).

Problem 2 – Delay interbed drainage

This problem simulates the drainage of a thick interbed caused by a step decrease in hydraulic head in the aquifer and is based on sample problem 1 in [Hoffmann and others \(2003\)](#). Because of the characteristically low vertical hydraulic conductivity of fine-grained silts and clays that constitute the interbeds, the equilibration of hydraulic heads in thick interbeds imbedded in an aquifer system typically lags head changes in the surrounding aquifer. Because the hydraulic gradient within the interbeds can be treated as vertical if the horizontal extents of the interbeds are much greater than their thicknesses, the delayed dissipation of unequilibrated heads within the interbeds can be described by the one-dimensional diffusion equation,

$$\frac{\partial^2 h}{\partial z^2} = \frac{S'_S}{K'_v} \frac{\partial h}{\partial t}, \quad (1)$$

where z is the vertical spatial coordinate (L), S'_S is the specific storage of the interbed (unitless), K'_v is the vertical hydraulic conductivity of the interbed (L/T), and t is time (T). The solution of this diffusion problem is identical to heat diffusion. [Carslaw and Jaeger \(1959\)](#) developed an analytical solution for heat diffusion from a slab with the ends at a constant temperature that can be recast to solve equation 1 for delayed flow from a thick interbed. If the initial head at $t = 0$ is h_0 throughout the thickness of the interbed (b_0), and the head in the surrounding aquifer is Δh above h_0 for $t > 0$, the head distribution [$h(z, t)$] for the interbed can be written as the infinite series

$$h(z, t) - h_0 = \Delta h - \frac{4\Delta h}{\pi} \sum_{k=0}^{\infty} \frac{-1^k}{2k+1} e^{-\frac{\pi^2}{4} \frac{t}{\tau_k}} \cos \left(\frac{(2k+1)\pi z}{b_0} \right), \quad (2)$$

where the time constant, τ_k , is defined as

$$\tau_k = \frac{\left(\frac{b_0}{2}\right)^2 S'_S}{(2k+1)^2 K'_v}. \quad (3)$$

In equation 2, $z = 0$ is assumed to be at the midplane of the interbed, with the boundaries at $\pm \frac{b_0}{2}$. Note that both the coefficients in the sum and the τ_k decrease as k increases. Thus, the true head distribution can be adequately described by a finite number of addends (k), particularly for later times. In the context of interbed compaction and land subsidence, the time delay caused by slow dissipation of transient overpressures is often given in terms of the time constant

$$\tau_0 = \frac{\left(\frac{b_0}{2}\right)^2 S'_S}{K'_v}, \quad (4)$$

which is the time during which about 93 percent of the ultimate compaction for a given decrease in head occurs ([Riley, 1969](#)). Because τ_0 is proportional to S'_S , which generally is much larger for inelastically deforming interbeds than for elastically deforming interbeds, deformation in elastically deforming interbeds is often assumed to occur instantaneously. The same is true for very thin inelastically deforming interbeds. Thus, equation 4 can be used to determine in which interbeds the time constant exceeds the model time step, necessitating consideration of use of delay-interbeds, which account for delayed drainage processes, instead of no-delay interbeds.

6 MODFLOW 6 CSUB Package Example Problems

Under constant geostatic stress conditions, compaction in the interbed can be directly related head changes using

$$\Delta b = S'_S \Delta h, \quad (5)$$

where Δb is the change in thickness of the interbed (L).

The model grid for this problem consists of 1 layer, 1 row, and 3 columns (fig. 3). The model has a top elevation of 0 meters and bottom elevation of -1,000 meters. DELR and DELC are equal to 1 meter. The simulation consists of one transient stress period 1,000 days in length, and is divided into 100 variable length time steps calculated using a time step multiplier equal to 1.05.

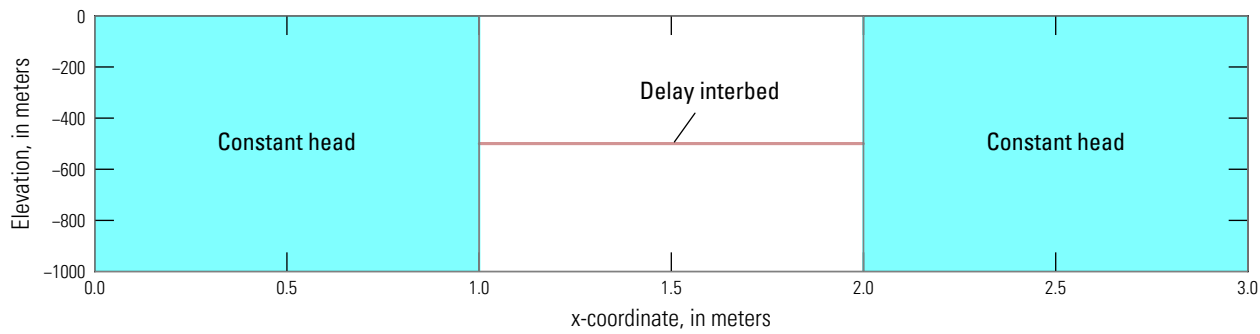


Figure 3. Model domain and setup for the delay interbed drainage problem. Interbed drainage is the result of step decrease in head in the aquifer.

The hydraulic conductivity in the aquifer was set to a very large value (1×10^6 meters per day), so that the head in the aquifer in the center cell remains constant. The specific yield and specific storage in the STO package were set to 0. Default flow property (NPF) and storage (STO) package settings were used. Initial heads were specified to be 0 meters.

Initially, the head-based formulation of the CSUB package was used to simulate compaction of the delay interbed and compare to analytical results calculated using equations 2 and 5. Ten finite-difference nodes represent the half-thickness of the interbed. The time constant, τ_0 (eq. 4), was chosen to be 1,000 with vertical hydraulic conductivity set to 2.5×10^{-6} meters per day, interbed thickness set to 1 meters, and elastic skeletal specific storage set to 1×10^{-5} per meter and inelastic skeletal specific storage set to 0.01 per meter. Meters and days units have been used in this problem but any consistent set of length and time units results in the same solution. The specific storage of coarse-grained aquifer material were specified to be 0×10^{-6} per meter. Water compressibility was not simulated in this problem and the thickness of compressible materials and total porosity were not updated during the simulation.

Constant-head cells, with a value of 0 meters, bound the delay interbed in column 2. The water released from the interbed during the simulation can leave the system through these constant-head cells. The starting head and the preconsolidation head in the delay interbed were specified to be 1 meter higher than the initial head in the surrounding aquifer.

The resulting compaction of the interbed is compared to the analytical solution (derived using equations 2, 4, and 5) in figure 3. The CSUB-computed values closely match the analytical values. The small differences, particularly at early times, may be at least partly due to the fact that the aquifer head in the simulation does not remain exactly constant as a result of water entering the aquifer from the interbed. Because of the finite transmissivity of the aquifer, the head in the aquifer briefly rises to about 2 percent of the starting head in the interbed during the first time step.

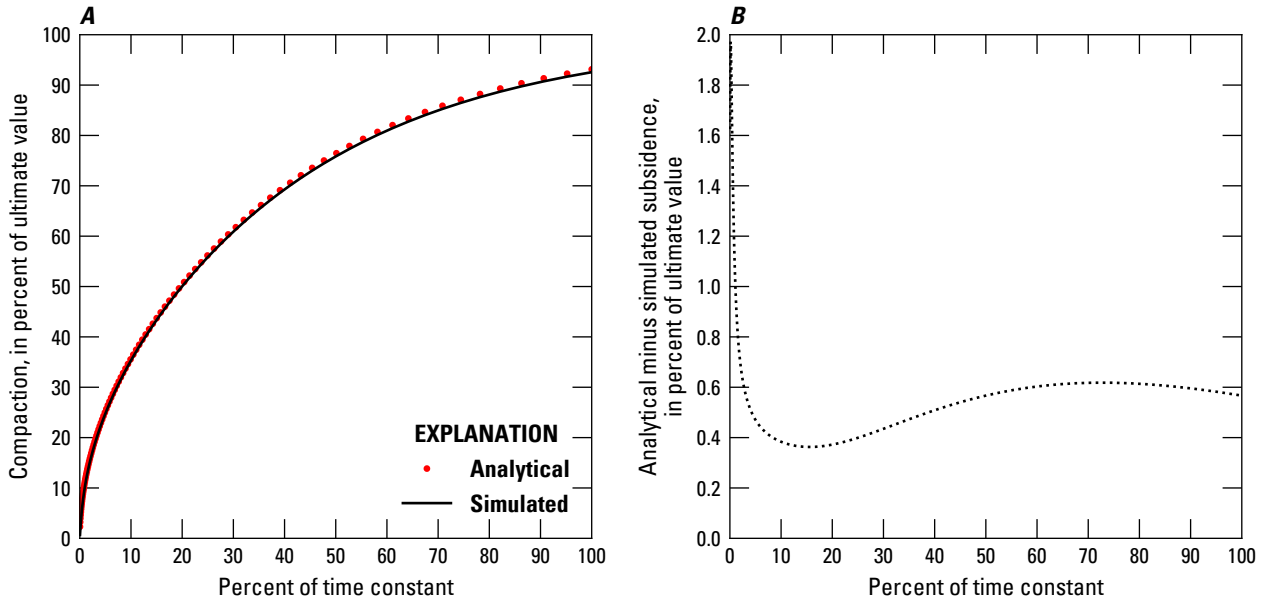


Figure 4. Graphs showing comparisons of simulated compaction with the head-based formulation and the analytical solution for the delay interbed drainage problem. *A*, comparison of the compaction history simulated with the analytical solution to the problem, and *B*, difference between the analytical solution and simulated compaction.

To evaluate differences between the head- and effective stress-based formulations, the problem shown in figure 3 was modified to use the effective stress-formulation. A total of 19 finite-difference nodes were used in the effective stress-based formulation so that results could be directly compared to the head-based formulation that used 10 finite-difference cells to represent the half-thickness of the interbed. A specific gravity of 1.7 and 2.0 was defined for moist and saturated sediments, respectively. The initial preconsolidation stress was set to be 1 meter less than the initial effective stress of 1,000 meters and is based on the initial preconsolidation head, which was defined to be 1 meter above the initial head in the head-based formulation.

The resulting effective stress-based compaction of the interbed is compared to the head-based solution in figure 5. The effective stress-based values closely match the head-based values. The small differences ($< 0.1\%$) are partly due to the fact that calculated specific storage values are not constant in the effective stress-formulation. Furthermore, the inelastic and elastic compression indices (41.8 and 4.18×10^{-2} (unit-less)), respectively), which are internally calculated from the initial effective stress and the user-provided inelastic and elastic specific storage values, results in a slightly smaller initial inelastic storativity value (9.5×10^{-3} versus 1.0×10^{-2}) that increase to values slightly larger than the user-provided inelastic storativity in subsequent time steps.

Another reason the difference between the head- and effective stress-based compaction shown in figure 5 is small is the interbed thickness is small (1 meter) and as a result the difference between the effective stress at the top and bottom of the interbed is also small. To evaluate the effect of the interbed thickness affects compaction, head- and effective stress-based models were run with interbed thicknesses ranging from 1 to 100 m. A time constant (τ_0) of 1,000 was used with elastic and inelastic skeletal specific storage values of 1×10^{-5} and 0.01 per meter, respectively, were used for each interbed thickness evaluated. The vertical hydraulic conductivity for each interbed thickness evaluated was calculated using equation 3 and the specified τ_0 and specific storage values. The calculated vertical hydraulic conductivity ranged from 2.5×10^{-6} to 0.025 meters per day for interbed thickness ranging from 1 to 100 meters, respectively. A total of 1,001 finite-difference nodes were used to simulate the interbed for the head- and effective stress-based formulation simulations to provide

8 MODFLOW 6 CSUB Package Example Problems

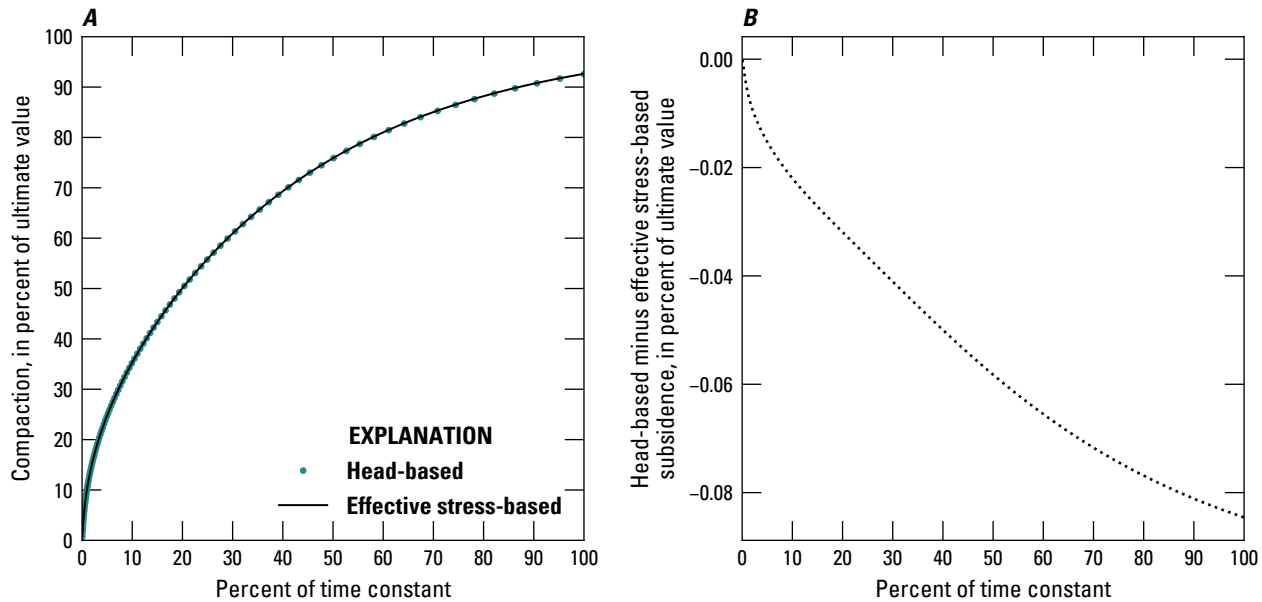


Figure 5. Graphs showing comparisons of simulated compaction for head- and effective stress-based formulations for the delay interbed drainage problem. *A*, comparison of the compaction history simulated with the head- and effective stress-based formulation solution to the problem, and *B*, difference between the simulated head- and effective stress-based formulation compaction.

additional spatial resolution for simulated interbed heads; the head-based simulations were simulated using a full-cell formulation. All other model parameters for the simulations that evaluated different interbed thicknesses were unchanged from the original values.

The difference between the analytical and simulated compaction and drainage rates at the top and bottom of the interbed relative to analytical drainage rates are shown in figure 6. The difference between head- and effective stress-based compaction for a 1 meter interbed thickness shown in figure 6A are identical to the results shown in figure 5B. In general, the differences between the simulated results and the analytical solution are comparable for interbed thickness less than 20 meters. Coincident with compaction differences, the average difference in drainage from the top and bottom of the interbed to the aquifer is greater than 0.7% (fig. 6B) for interbed thicknesses greater than 10 meters as a result of larger differences in the effective stress at the top and bottom of the interbed. The average difference between the effective stress at the bottom and top of the interbed is 2.02%, 5.13%, and 10.5% of the average interbed effective stress for the simulations with 20, 50, and 100 meters interbed thicknesses, respectively.

Figure 7 shows the vertical distribution of the difference in head- and effective stress-based formulation interbed heads relative to head-based interbed heads for each of the interbed thicknesses evaluated. Head-based interbed heads are symmetric about the center line of the interbed, with lower heads at the top and bottom of the interbed and the highest heads at the center of the interbed. As a result, negative and positive differences shown in figure 7 represent higher and lower interbed heads in the effective stress-based formulation than the head-based formulation, respectively. Generally, effective stress-based interbed heads are higher and lower in the top and bottom halves of the interbed, respectively, and differences are greatest for interbed thicknesses greater than 10 meters. The spatial distribution of interbed head differences is controlled by the decrease in the inelastic specific storage value resulting from the increase in effective stress with depth and the reduction in the water released from storage with depth in the interbed, which results in increased head changes with depth with the effective stress-formulation. As the simulation progresses, differences propagate from the top and bottom of interbed into the interbed as the maximum difference decreases.

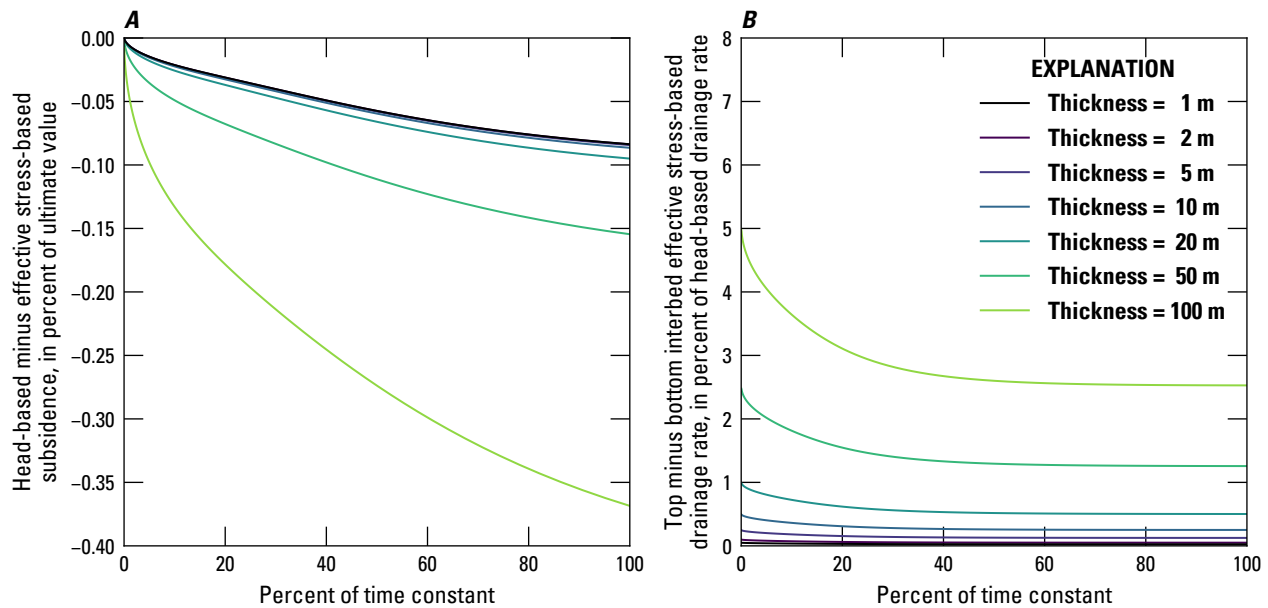


Figure 6. Graphs showing the difference between head- and effective stress-based compaction for different interbed thicknesses for the delay interbed drainage problem. *A*, difference between the head- and effective stress-based formulation compaction, and *B*, difference between drainage at the top and bottom of the interbed relative to the head-based formulation interbed drainage.

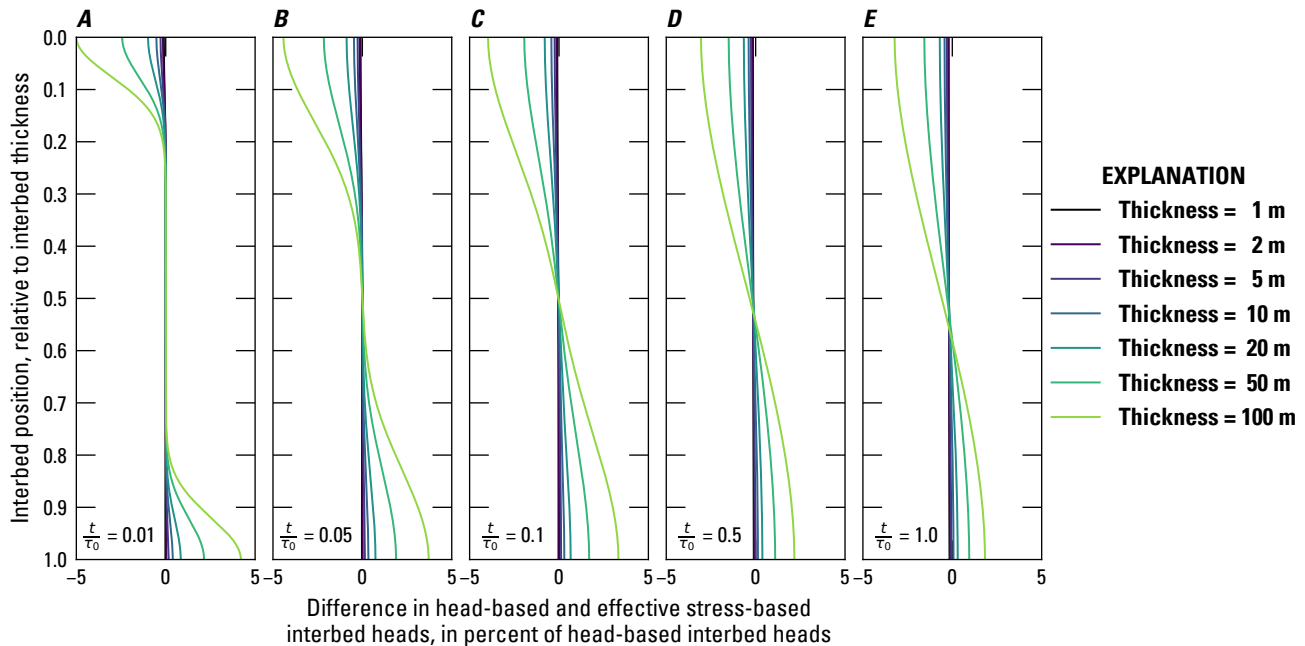


Figure 7. Graphs showing differences between head- and effective stress-based formulation interbed heads relative to head-based interbed heads for variable interbed thicknesses at select fractions of the time constant (τ_0) for the delay interbed drainage problem. *A*, 1 percent of τ_0 , *B*, 5 percent of τ_0 , *C*, 10 percent of τ_0 , *D*, 50 percent of τ_0 , and *E*, 100 percent of τ_0 .

10 MODFLOW 6 CSUB Package Example Problems

Problem 3 – One-dimensional compaction

A one-dimensional MODFLOW 6 model was developed by Sneed (2008) to simulate aquitard drainage, compaction and, land subsidence at the Holly site, located at the Edwards Air Force base, in response to effective stress changes caused by groundwater pumpage in the Antelope Valley in southern California (fig. 8). Land subsidence resulting from groundwater level declines, has long been recognized as a problem in Antelope Valley, California. The original one-dimension compaction model was calibrated to extensometer data from the USGS Holly site (station name 008N010W01Q005S) for the period from 1990 to 2006, and used a head based-formulation to represent compaction. The model of Sneed (2008) has been modified to use the effective stress formulation available in the CSUB package for MODFLOW 6.

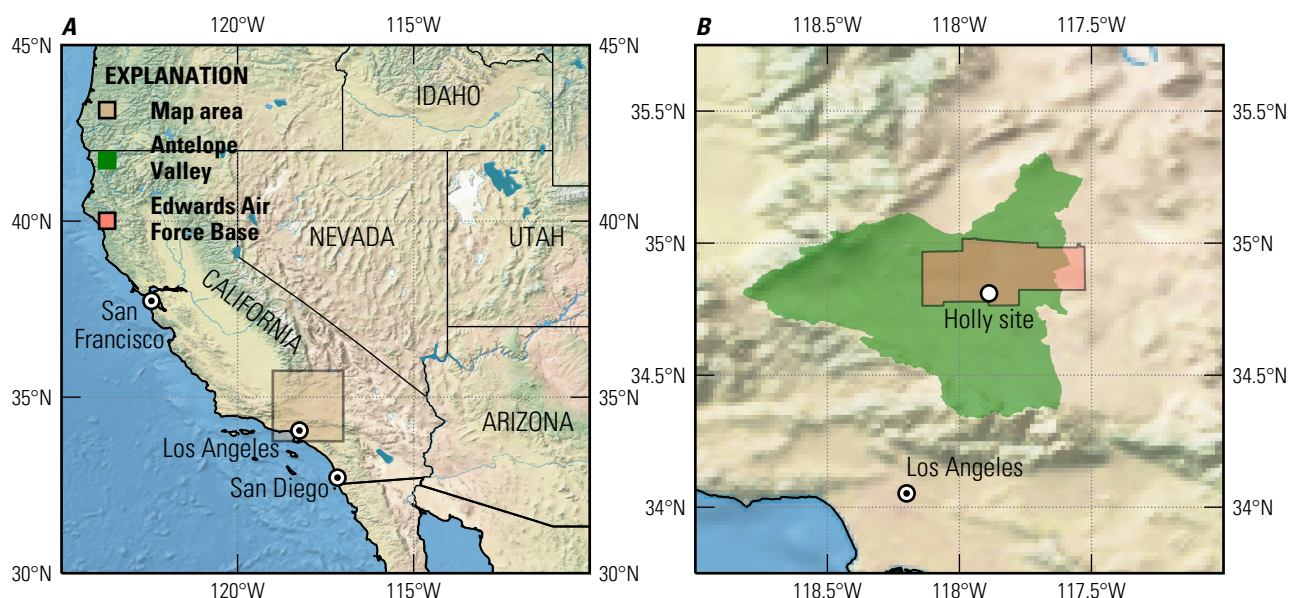


Figure 8. Maps showing the location of the study area for the one-dimensional compaction problem in southern California. *A*, location of the study area in southern California and *B*, location of the Holly site and Edwards Air Force Base in the Antelope Valley. Cross-blended hypsometric tints with relief, water, drains and ocean bottom background image from Natural Earth and is available at <https://www.naturalearthdata.com/downloads/50m-raster-data/50m-cross-blend-hyps/>, accessed on July 9, 2019.

The subsurface geology at the Holly site comprises Quaternary alluvial and lacustrine deposits from land surface to about 260 meters below land surface, consolidated late Tertiary and early Quaternary sedimentary continental deposits from about 260 to 330 meters below land surface, and decomposed basement complex. Lithologic and geophysical logs of the Holly site indicate the presence of relatively thin interbedded aquitards, ranging from 0.3 to 5 meters thick, and two thicker aquitards 20 meters (37–57 meters below land surface) and 19 meters (92–111 meters below land surface) thick. The upper aquitard is interpreted as a regionally extensive, confining unit. The groundwater system at the Holly site is comprises two aquifer systems—an unconfined system and a confined system, which are separated by lacustrine blue-clay deposits that constitute the confining unit. The upper aquifer is unconfined, about 37 meters thick and the water table is about 20 meters below land surface. The confined-aquifer system at the site extends about 275 meters below the confining unit, where it is underlain by weathered bedrock. The middle aquifer is the source of most of the groundwater pumped from the well field closest to the Holly site. Additional information on the hydrogeology of the Holly site and the Antelope Valley can be found in Sneed and Galloway (2000) and Sneed (2008).

Compaction at the Holly site for the period from 1990 through 2006 was measured using a counter-

weighted pipe extensometer designed to measure compaction in the interval from 4.6 to about 260 meters below land surface. The principal mode of compaction at the Holly site is a seasonally dependent step response. Larger rates of compaction are associated with summer water-level drawdowns and despite ground-water level recoveries of more than 3 meters during the winter, compaction continues, at a reduced rate. The absence of aquifer-system expansion during seasonal water-level recovery is consistent with the delayed drainage and resultant delayed, or residual, compaction of thick aquitards.

The model grid for this problem consists of 14 layers, 1 row, and 1 column (fig. 9). The model layers are based on the model of Sneed (2008), with the exception of the top of model layer 1 which was modified from the original value of -27.74 meters to 0 meters to allow the model to account for unsaturated conditions above the water table when calculating geostatic and effective-stresses. Model layer thicknesses are summarized in table 3. DELR and DELC are equal to 1 meter. The model consists of 353 stress periods covering the period from May 8, 1908 to September 4, 2006. The duration of model stress periods and time steps for the period from May 8, 1908 to May 9, 1990 (“early time”) were annual and monthly—365.25 and 30.4375 days, respectively, and were 22 and 1 days, respectively, for the period from May 9, 1990 to September 4, 2006 (“late time”). The nearly century duration of the simulations allows for comparisons of aquifer-system compaction owing to sustained groundwater pumpage and water-level declines through the period of groundwater development and seasonal groundwater level cycling since 1990.

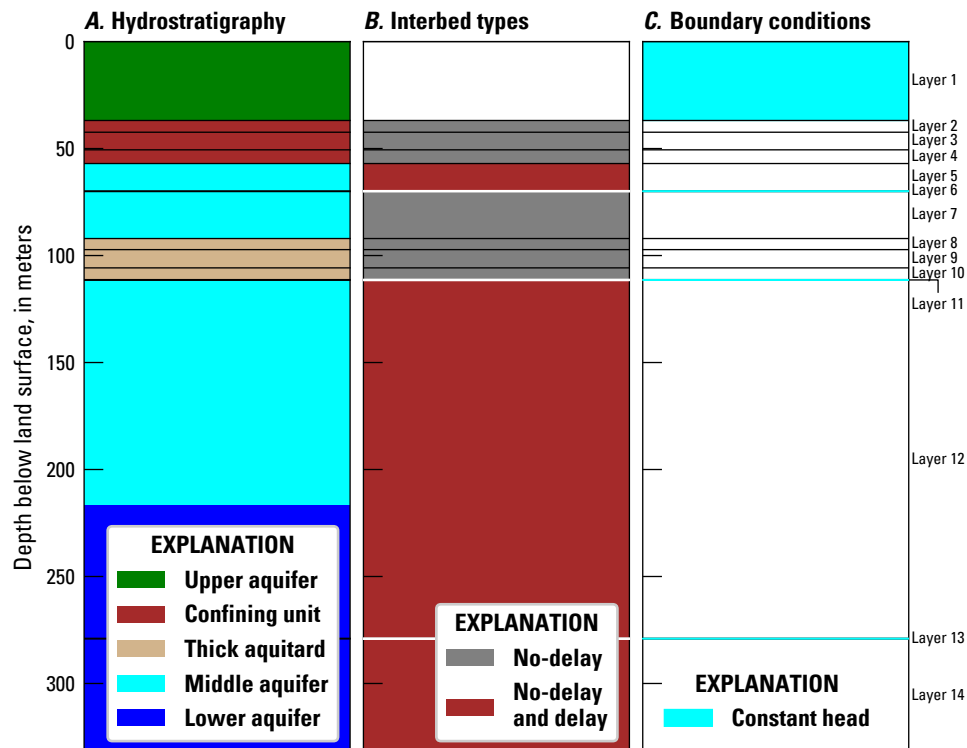


Figure 9. Diagram showing the model domain and setup for the one-dimensional compaction problem. *A*, hydrostratigraphy, *B*, interbed types used in aquifer and confining units, and *C*, location of constant-head boundary conditions.

Hydraulic properties used in the model are shown in table 3 and are identical to properties used by Sneed (2008). The specific yield and specific storage in the STO package were defined to be 0 for all layers. All model layers are defined to be non-convertible for hydraulic conductivity and storage properties. Default NPF and STO package settings were used. Initial heads in the model range from 0. to 6.77 meters (table 3).

The effective stress formulation of the CSUB package was used to simulate compaction of aquifer materials. Fine-grained materials defined as delay interbeds were discretized using 39 cells and assigned a

12 MODFLOW 6 CSUB Package Example Problems

Table 3. Aquifer system thickness and hydraulic properties for the one-dimensional compaction problem.

Model layer	Layer thickness, in meters	Horizontal hydraulic conductivity, in meters per day	Vertical hydraulic conductivity, in meters per day	Initial head, in meters
1	36.88	7.56×10^{-5}	9.14×10^{-3}	0.00
2	5.49	5.08×10^{-4}	3.66×10^{-6}	1.57
3	8.23	3.39×10^{-4}	3.66×10^{-6}	3.38
4	6.40	4.35×10^{-4}	3.66×10^{-6}	5.56
5	12.80	2.18×10^{-4}	9.14×10^{-3}	6.77
6	0.30	9.14×10^{-3}	9.14×10^{-3}	6.77
7	21.95	1.27×10^{-4}	9.14×10^{-3}	6.77
8	5.18	5.38×10^{-4}	4.57×10^{-6}	6.77
9	8.53	3.27×10^{-4}	4.57×10^{-6}	6.77
10	5.49	5.08×10^{-4}	4.57×10^{-6}	6.77
11	0.30	9.14×10^{-3}	9.14×10^{-3}	6.77
12	167.34	1.67×10^{-5}	9.14×10^{-3}	6.77
13	0.30	9.14×10^{-3}	9.14×10^{-3}	5.55
14	53.34	5.23×10^{-5}	9.14×10^{-3}	5.55

uniform vertical hydraulic conductivity of 4.57×10^{-6} meters per day. A specific gravity of 1.7 and 2.0 was defined for moist and saturated sediments, respectively. Water compressibility was simulated using a specific gravity of water of 9,806.65 Newtons per cubic meters and water compressibility of 4.6512×10^{-10} per Pascal. The thickness of compressible materials and total porosity were updated during the simulation in response compaction.

Interbedded aquitards ranged from 0.3 to 5.5 meters in thickness. The Holly model simulates interbedded aquitards less than 1.5 meters thick using no-delay interbeds (ultimate compaction occurs within a model time step), and simulates interbedded aquitards 1.5 meters thick or greater using delay-interbeds (ultimate compaction does not occur within a model time step). A total of 18 interbedded aquitards ranging from approximately 0.3 to 1.2 meters thick, with a total aggregate thickness of approximately 12 meters, were modeled as no-delay interbeds and 10 interbedded aquitards ranging from approximately 1.5 to 5.5 meters thick, with a total aggregate thickness of approximately 27 meters, were modeled as delay interbeds. The confining unit (approximately 20 meters thick) and the thick aquitard (approximately 19 meters thick), were modeled as no-delay interbeds. Simulation of delayed drainage and residual compaction in each of these units was simulated implicitly using 3 model layers as recommended in [Hoffmann and others \(2003\)](#). Compaction was not simulated for the upper aquifer because the upper aquifer is relatively coarse grained and heads are changing very slowly and are hydraulically isolated from seasonal groundwater fluctuations in the production zones of the aquifer system. A constant porosity of 0.30 was used for the coarse- and fine-grained materials in the model.

Initial preconsolidation stresses were calculated from initial preconsolidation heads developed by [Sneed \(2008\)](#) and effective stresses calculated using initial heads (table 3). Initial preconsolidation stresses for no-delay and delay interbeds are summarized in tables 5, respectively. [Sneed \(2008\)](#) estimated initial preconsolidation heads from the time series for paired bench marks near the Holly site and middle aquifer water levels (fig. 10). Delay beds in the middle aquifer (model layers 5 and 12) and the lower aquifer (model layer 12) were specified to be 6.77 and 5.55 meters above land surface, respectively, which are the same as initial heads in these layers.

Boundary conditions in the one-dimensional compaction model of the Holly site consist of constant (time-

variant) heads for those parts of the coarse-grained aquifer that represent measured (or estimated) hydraulic head (fig. 9C). The upper, middle, and lower aquifers at the Holly site are represented in the model by specifying heads in each aquifer using data from Sneed (2008) and are shown in figure 10. The upper model boundary is a time-variant, constant-head boundary that represents measured or estimated heads in the upper aquifer (model layer 1) at the Holly site and is about 28 meters below land surface (fig. 9C). Three boundaries within the model domain consist of time-variant, specified heads that represent measured or estimated heads in the middle (model layers 6 and 11) and lower aquifers (model layer 13) at the Holly site (fig. 9C). Time-varying heads for constant-head cells were defined using a time series file. Although compaction is not thought to be important in the upper aquifer it should be noted that compaction and related release/storage of water are not simulated in cells with constant-head boundaries.

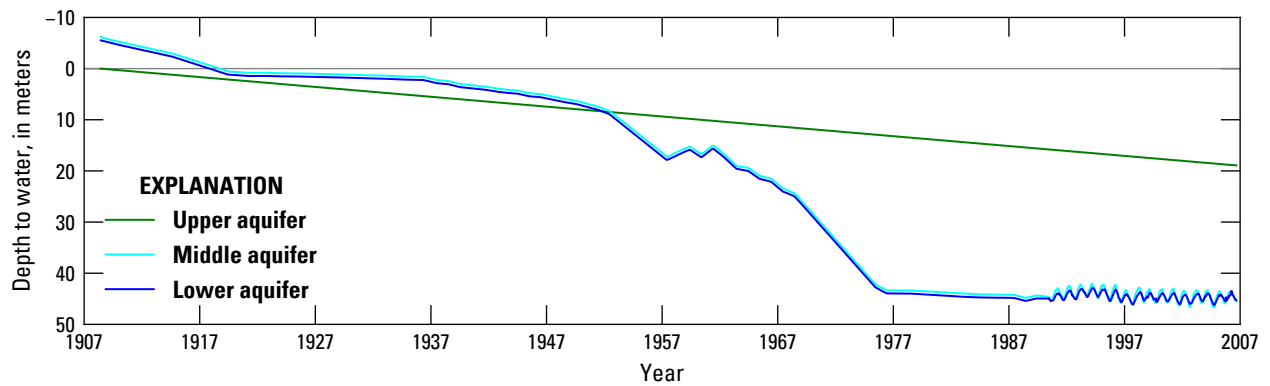


Figure 10. Graph showing depth to water values used in the one-dimensional compaction problem for the upper, middle, and lower aquifers at the Holly site, Edwards Air Force Base, Antelope Valley, California. Modified from Sneed (2008).

The compaction at the end of the simulation for the confining unit (0.28 meters), the thick aquitard (0.66 meters), no-delay interbeds contained in aquifer units (0.06 meters), delay interbeds contained in aquifer units (0.35 meters), and coarse grained materials (0.06 meters) from a modified MODFLOW 6 version of the model of Sneed (2008) were used to calibrate initial specific storage values used in the model. The specific storage values used by Sneed (2008) were uniformly scaled by a factor of 9.9408×10^{-1} to better match the observed compaction at the Holly site for the period from October 1, 1992 to May 9, 2006. The total compaction at the end of the simulation period (1.42 meters) and the total compaction from October 1, 1992 to May 9, 2006 (0.19 meters) were also used to calibrate initial specific storage values used in the model.

PEST++ (Welter and others, 2015) was used to calibrate 1) the elastic specific storage value for coarse grained materials in model layers 5, 7, 12, and 14; 2) inelastic and elastic specific storage values for the confining unit (model layers 2–4); 3) inelastic and elastic specific storage values for the thick aquitard (model layers 8–10); and 4) inelastic and elastic specific storage value were calibrated for no-delay and delay interbeds contained in aquifer units (model layers 5, 6, 12, and 14). Compaction values simulated using the head-based formulation for the confining unit, the thick aquitard, no-delay interbeds contained in aquifer units, delay interbeds contained in aquifer units, and coarse grained materials were given a weight of 1; total compaction and the total compaction from October 1, 1992 to May 9, 2006 were given an increased weight of 5 to favor fitting the total compaction and observed change in total compaction over material based compaction values.

Comparison of head- and effective stress-based compaction results are shown in figure 11. The compaction at the end of the simulation in the model using head- and effective stress-based formulation were essentially identical and mean errors calculated for the entire simulation ranged from -0.0045 meters (confining unit compaction) to 0.0042 meters (compaction in delay interbeds contained in aquifer units), with the largest differences occurring between approximately 1947 and 1977.

14 MODFLOW 6 CSUB Package Example Problems

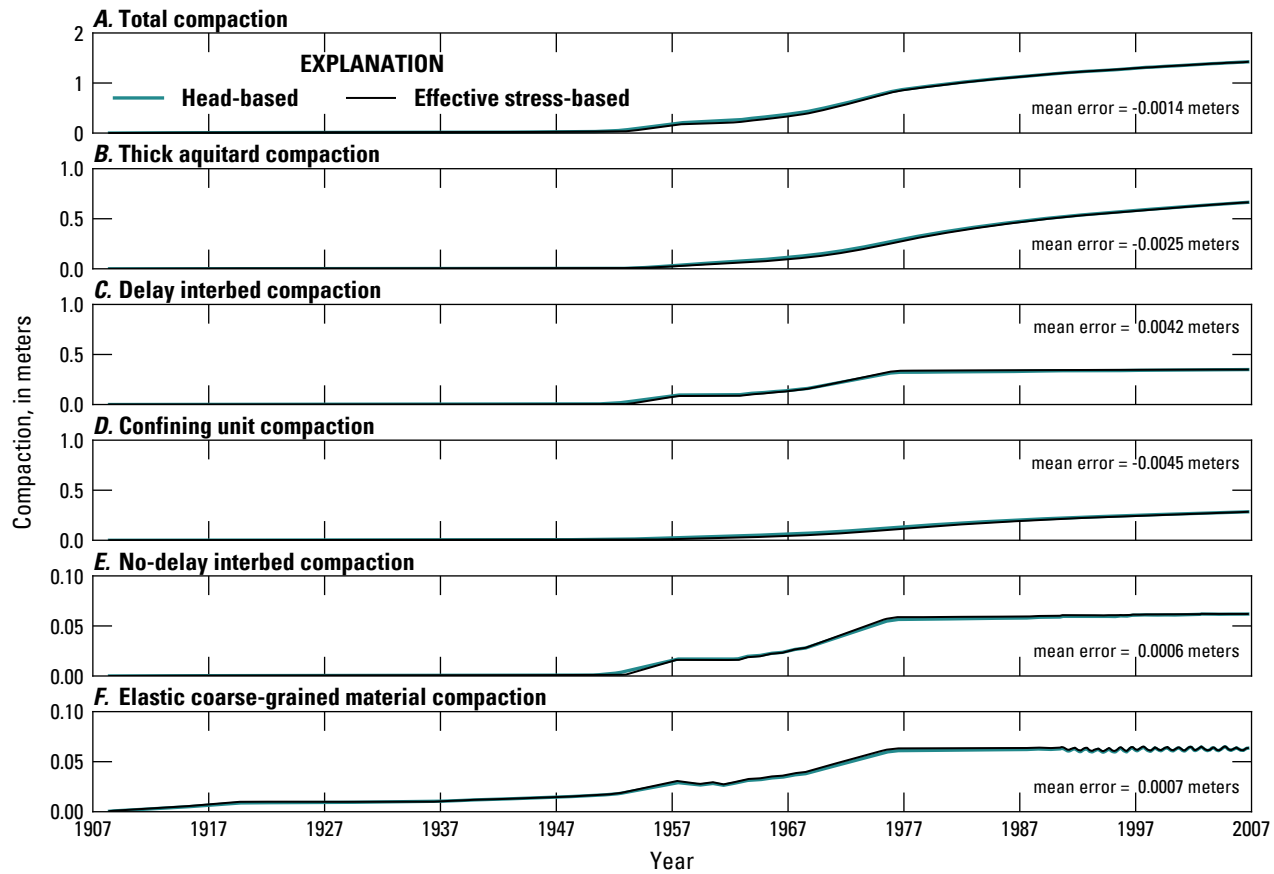


Figure 11. Graphs showing simulated compaction in different material types using head- and effective stress based formulations for the one-dimensional compaction problem. *A*, Total compaction, *B*, compaction in interbeds in the thick aquitard, *C*, compaction in delay interbeds contained in aquifers, *D*, compaction in interbeds in the confining unit, *E*, compaction in no-delay interbeds contained in aquifers, and *F*, compaction in coarse-grained materials.

The thickness of compressible materials and calibrated specific storage values for coarse-grained materials, fine-grained materials represented as no-delay interbeds, and fine-grained materials represented as delay interbeds are summarized in tables 4 and 5, respectively. Calibrated specific storage values are larger than values used with the head-based formulation. Percent differences relative to values used by Sneed (2008) were 27.0% for the elastic specific storage values of coarse-grained materials, averaged 79.2 and 210.2% for the inelastic and elastic specific storage values of no-delay interbeds, and averaged 20.6 and 52.2% for the inelastic and elastic specific storage values of delay interbeds. Larger specific storage values are expected for the effective stress-based formulation since effective-stress values increase during the simulation, as a result of groundwater pumpage induced water-level declines, and result in reduced specific storage values and compaction with time relative to the head-based formulation model using the uniformly scaled specific storage values from Sneed (2008).

The simulations for the period 1908–2006 provide information about how the aquifer-system components, aquifers and aquitards, contributed to overall compaction because of the continual lowering of water levels throughout the 1900s and because of seasonal water-level cycling since 1990. Simulated compaction totaled 1.42 meters for the period 1908–2006. Of the total simulated compaction, the confining unit (thickness = 20.12 meters) accounted for 20.0% of the total; the thick aquitard (thickness = 19.20 meters) accounted for 46.7% of the total; delay interbeds in aquifers (aggregate thickness = 18.14 meters) accounted for 24.6%; coarse-grained materials (aggregate thickness = 225.39 meters) accounted for 4.5% of the total; and no-delay

Table 4. Coarse-grained material thickness and hydraulic properties for the one-dimensional compaction problem.

Model layer	Thickness, in meters	Specific storage, in per meter
5	4.79	6.39×10^{-7}
7	21.34	6.39×10^{-7}
12	154.66	6.39×10^{-7}
14	44.61	6.39×10^{-7}

Table 5. Fine-grained material no-delay and delay interbed thickness and hydraulic properties for the one-dimensional compaction problem. Equivalent interbed thickness and delay interbed material factor values are defined for delay interbeds..

Interbed number	Model layer	Interbed thickness, in meters	Equivalent interbed thickness, in meters	Delay interbed material factor, unitless	Inelastic specific storage, in per meter	Elastic specific storage, in per meter	Initial preconsolidation stress, in meters
1	2	5.49			1.26×10^{-4}	7.96×10^{-7}	47.27
2	3	8.23			1.26×10^{-4}	7.96×10^{-7}	55.93
3	4	6.40			1.26×10^{-4}	7.96×10^{-7}	62.76
4	5	2.74			2.50×10^{-5}	1.17×10^{-6}	75.90
5	7	0.61			2.52×10^{-5}	1.07×10^{-6}	98.15
6	8	5.18			1.79×10^{-4}	3.18×10^{-6}	103.33
7	9	8.53			1.79×10^{-4}	3.18×10^{-6}	111.86
8	10	5.49			1.79×10^{-4}	3.18×10^{-6}	117.35
9	12	7.62			1.36×10^{-5}	5.94×10^{-7}	285.60
10	14	0.91			2.01×10^{-5}	8.59×10^{-7}	339.25
11	5	5.27	2.74	1.92	2.11×10^{-5}	9.56×10^{-7}	75.90
12	12	5.06	3.05	1.66	4.52×10^{-5}	7.05×10^{-7}	285.60
13	14	7.82	2.74	2.85	9.45×10^{-5}	6.38×10^{-7}	339.25

interbeds in aquifers (aggregate thickness = 11.89 meters) accounted for 4.4% of the total (fig. 12A). During 1990–2006, a total of 0.23 meters of compaction was simulated; the confining unit accounted for 31.2% of the total; the thick aquitard accounted for 66.3% of the total; delay interbeds in aquifers accounted for 1.7%; coarse-grained materials accounted for -0.1% (representing expansion of coarse grained materials); and no-delay interbeds in aquifers accounted for 0.9% of the total. For these relatively quickly equilibrating thin aquitards, the fairly stable stresses since the mid-1970s and cyclic stresses during the late time were often in the elastic range of stress. In fact, beginning in about 1976, the delay and no-delay interbeds in aquifers had significantly reduced compaction rates, contributing only 0.01 meters (2.4%) and 0.004 meters (0.1%) of compaction, respectively, during the last 30 years of the simulation. These thin aquitards deformed mostly elastically during the late time (fig. 12).

The simulated stress/displacement trajectory also compares well in magnitude and timing with the measured stress/displacement trajectory between October 1, 1992 and September 4, 2006 (fig. 12C). The effective stress at the base of the lower aquifer was estimated using water-level data for the upper and lower aquifers (fig. 10). The estimated stress/displacement trajectory fit is poorest from 1993 to 1996 when seasonal compaction changes lag behind observed changes. After April 1997, simulated compaction is generally consistent with observed compaction.

Vertical distributions of hydraulic head in the aquitards can be used as a direct measure of residual com-

16 MODFLOW 6 CSUB Package Example Problems

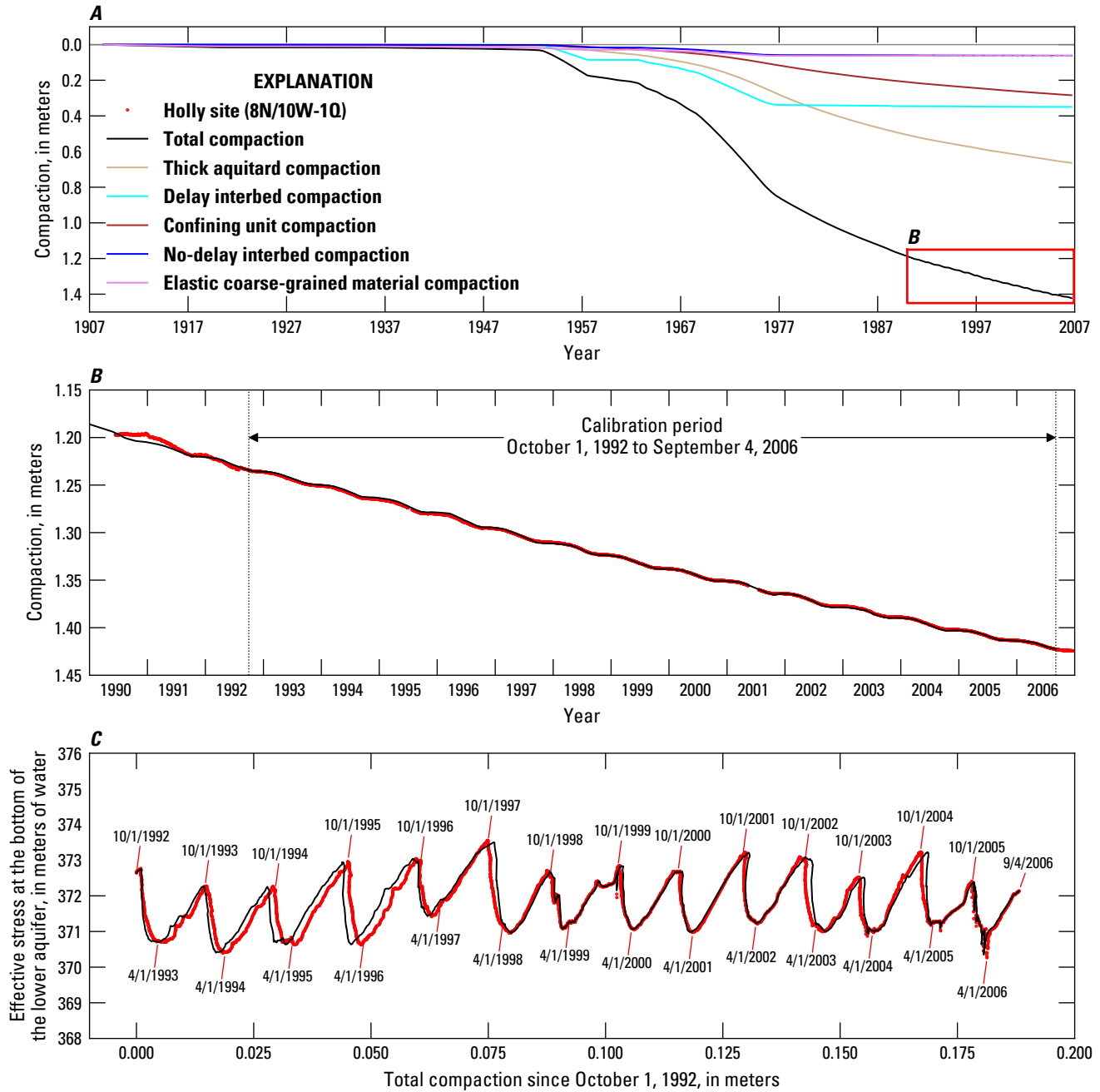


Figure 12. Graphs showing history matches for simulated and measured aquifer-system compaction in the one-dimensional compaction problem. *A*, compaction in the different material types for the full simulation period (for 1908–2006), *B*, comparison of simulated and observed compaction at the Holly site for the period from 1990 to 2007, and *C*, simulated and observed stress/displacement for the period from October 1, 1992 to September 4, 2006. Elastic and inelastic specific storage values were calibrated using observed Holly site compaction data for the period from October 1, 1992 to September 4, 2006 and simulated compaction from the model based on [Sneed \(2008\)](#), which used a head-based formulation to simulate compaction.

compaction ([Riley, 1969, 1998](#)). A linear profile showing deviations in the simulated 1908 to 2006 head distributions for the two thick clay sequences—the confining unit and the thick aquitard—indicate large residual excess pore pressures exist at the end of the simulation (fig. 13). Residual excess pore pressures in these thick aquitards began accumulating in about 1950, when water levels in the aquifers began declining at rate faster (fig. 10) than these aquitards could dissipate excess pore pressures. The simulations indicate that about 98% of

the compaction during late time is residual compaction occurring in these two thick clay sequences (fig. 12A).

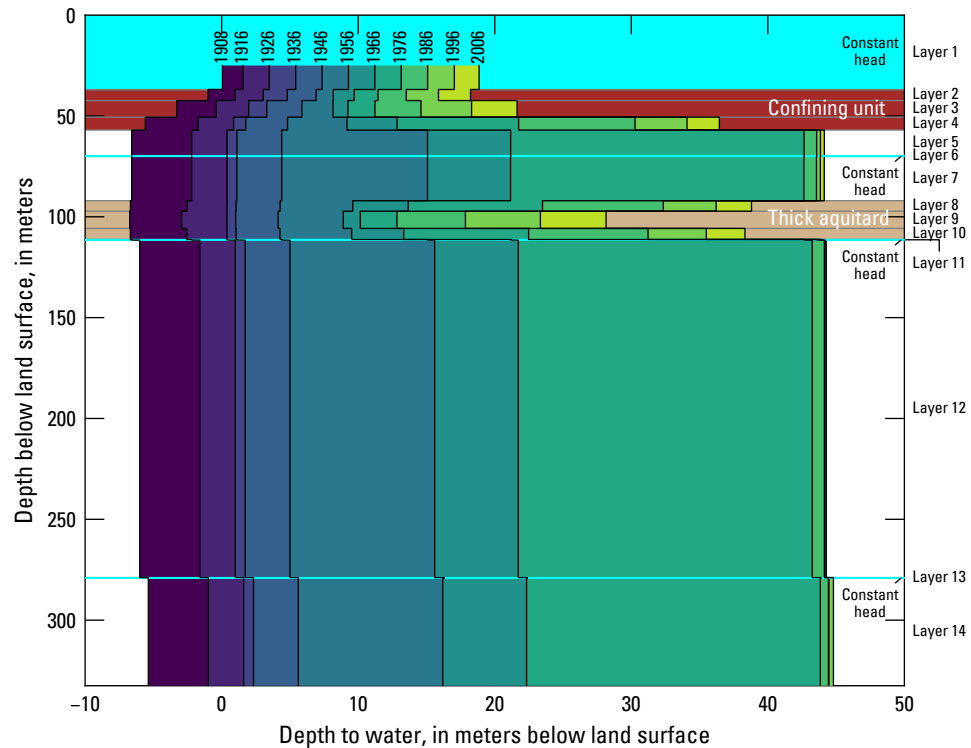


Figure 13. Graph showing simulated vertical head profiles and approximately decadal head changes in the one-dimensional compaction problem. Vertical head profiles are shown for 1908, 1916, 1926, 1936, 1946, 1956, 1966, 1976, 1986, 1996, and 2006. The colored area between plotted years represents the simulated head change over approximately decadal period of time between simulated vertical head profiles. The vertical location of model layer tops and bottom and layers with constant-head boundaries are also shown..

Problem 4 – One-dimensional compaction in a three-dimensional flow field

This problem is based on the problem presented in the SUB-WT report (Leake and Galloway, 2007) and represent groundwater development in a hypothetical aquifer that includes some features typical of basin-fill aquifers in an arid or semi-arid environment. The problem of Leake and Galloway (2007) was modified to include compaction of coarse-grained aquifer materials and water compressibility. Specific stress packages were also modified but net inflows to the model domain are identical.

The model grid for this problem consists of four layers, 20 rows, and 15 columns (fig. 14). The model has a top elevation of 150 meters and layer bottom elevations of 50, -100, -150, and -350 meters for layers 1, 2, 3, and 4, respectively. DELR and DELC are specified with a constant value of 2,000 meters. The simulation consists of three stress periods. The first is an initial steady-state period for the purpose of computing the head distribution, which is used with other quantities to compute the initial hydrostatic, effective, geostatic, and pre-consolidation stresses. The second stress period is used to simulate 60 years of pumping by the two wells at locations shown in figure 14. The third stress period is used to simulate 60 years of recovery following cessation of pumping. The second and third stress periods are divided into 60, 1-year time steps.

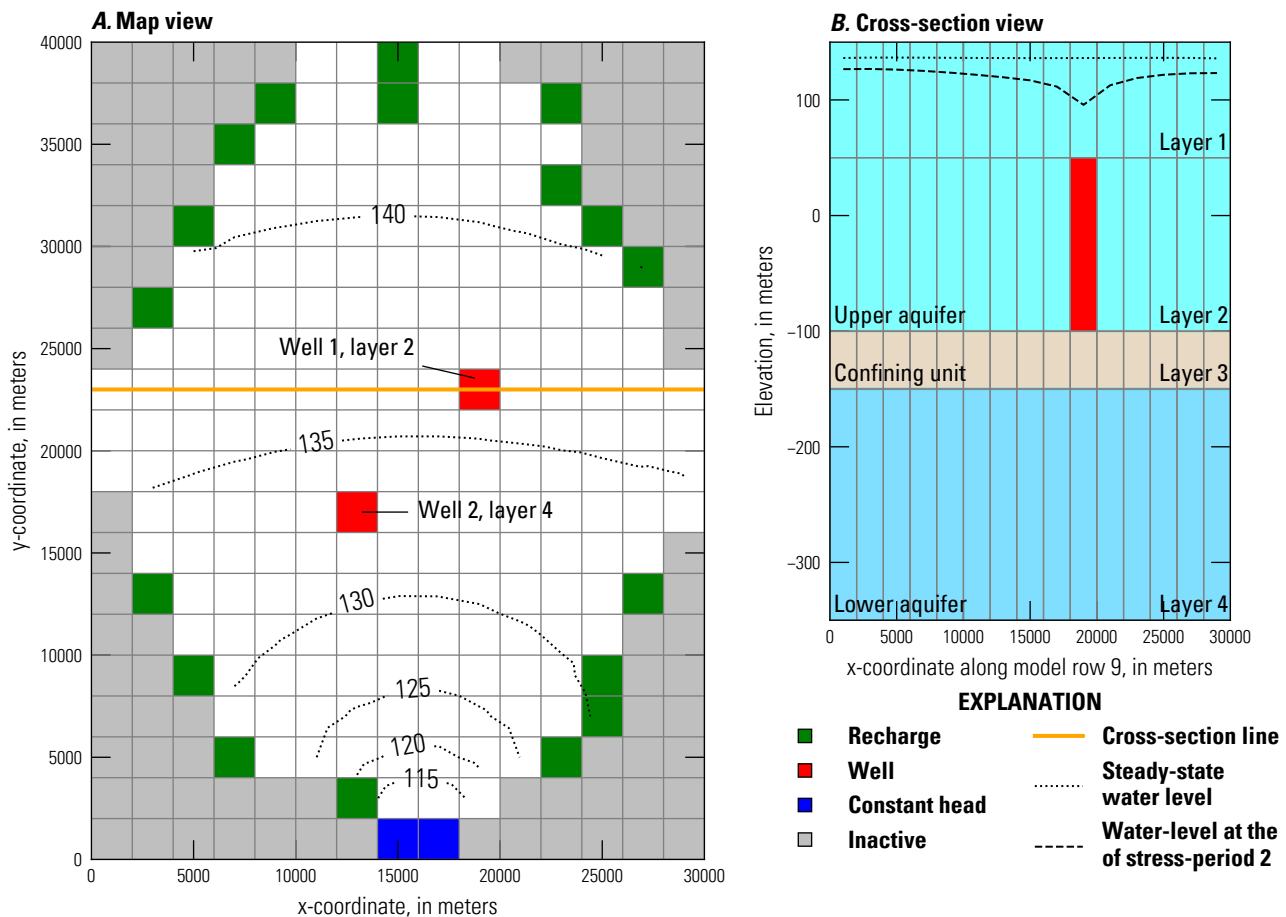


Figure 14. Diagram showing the model domain for the one-dimensional compaction in a three-dimensional flow field problem. A, plan view, and B, cross-section view. The locations of active and inactive areas of the model domain, steady-state heads in model layer 1, and locations of recharge cells, constant-head cells, and wells are also shown.

The aquifer system consists of an unconfined upper aquifer, an extensive confining unit, and a confined lower aquifer (fig. 14B). The model uses two layers to represent the water-table aquifer and one layer each to

represent the confining unit and the lower aquifer. Hydraulic conductivity was assumed to be isotropic in the horizontal and vertical directions in each layer. Hydraulic properties for coarse-grained materials are listed in table 6. The specific storage was defined to be 0 for all layers in the STO package. Model layer 1 and layers 2–4 were defined to be convertible and non-convertible, respectively, for hydraulic conductivity and storage properties. Default NPF and STO package settings were used. An initial head of 100 meters was defined for each layer.

Table 6. Coarse-grained material hydraulic properties for the one-dimensional compaction in a three-dimensional flow field problem.

Layer	Cell thickness, in meters	Horizontal hydraulic conductivity, in meters per day	Vertical hydraulic conductivity, in meters per day	Total porosity, unitless	Specific yield, unitless	Recompression index, unitless
1	100	4	0.4	0.32	0.30	0.005
2	150	4	0.4	0.32	0.30	0.005
3	50	0.01	0.01	0.45	0.40	0.010
4	200	4	0.4	0.32	0.30	0.005

The effective stress formulation of the CSUB package was used to simulate compaction of aquifer materials. Storage properties for coarse- and fine-grained materials were specified using compression indices. No-delay interbeds were specified in each active model cell. Hydraulic properties for fine-grained materials represented as no-delay interbeds are listed in table 7; no-delay interbeds in model 3 comprise the full thickness of the confining unit.

Table 7. Fine-grained material hydraulic properties for the one-dimensional compaction in a three-dimensional flow field problem.

Layer	Interbed thickness, in meters	Total porosity, unitless	Compression index, unitless	Recompression index, unitless
1	45	0.45	0.25	0.010
2	70	0.45	0.25	0.010
3	50	0.45	0.25	0.010
4	90	0.45	0.25	0.010

The specific gravity of fully- and partially-saturated materials for each layer was calculated using

$$G = (1 - \bar{\theta})G_{\text{solid}} + k_r \bar{\theta} G_{\text{water}}, \quad (6)$$

where G is the specific gravity of a control volume that includes solids and water (unitless), $\bar{\theta}$ is the thickness weighted porosity of coarse- and fine-grained materials in a control volume (unitless), G_{solid} is the specific gravity of the solids in a control volume (unitless), k_r is a scaling factor used to scale the specific gravity of water if a control volume is not fully saturated (unitless), and G_{water} is the specific gravity of water (unitless). k_r is 1 for saturated materials or the ratio of the volume of water to the total volume for materials that are not fully saturated.

20 MODFLOW 6 CSUB Package Example Problems

The specific gravity of saturated materials for each layer was calculated using the thickness weighted porosity listed in table 8, a G_{solid} value of 2.7, and a G_{water} value of 1.0. The specific gravity of moist materials was calculated using a k_r value of 0.25 and the other values used to calculate the specific gravity of saturated materials. The specific gravity of saturated and moist materials used for the one-dimensional compaction in a three-dimensional flow field problem are listed in table 8

Table 8. Specific gravity of saturated and moist materials for the one-dimensional compaction in a three-dimensional flow field problem.

Layer	Thickness weighted porosity, unitless	Specific gravity of saturated materials, unitless	Specific gravity of moist materials, unitless
1	0.3785	2.06	1.77
2	0.3807	2.05	1.77
3	0.4500	1.94	1.60
4	0.3785	2.06	1.77

Water compressibility was simulated and default specific gravity of water ($\gamma_{\text{water}} = 4.6512 \times 10^{-10}$ per Pascal) and the compressibility of water ($\beta = 9806.65$ Newtons per cubic meter) values were used. Initial specific storage values related to the compressibility of water ($S_{s_{\text{water}}} = \theta\beta\gamma_{\text{water}}$) were 1.46×10^{-6} and 2.05×10^{-6} per meter for coarse- and fine-grained materials, respectively. The porosity and thickness of coarse- and fine-grained materials were adjusted during the simulation in response to compaction. The initial preconsolidation stress for the no-delay interbeds was specified to be 15 meters greater than the steady-state effective stress calculated in each cell at the end of stress period 1.

Inflow to the flow system is simulated using the recharge package at 18 recharge locations in layer 1 shown on figure 14A. Recharge at each of these locations is specified at a rate of 5.5×10^{-4} meters per day throughout the entire simulation, resulting in a total recharge rate of 39,600 cubic meters per day. Under steady-state conditions, all of the flow leaves the system through eight constant-head cells, two of which are in each layer at the horizontal locations shown on figure 14A. Head at the eight constant-head cells is specified to be 100 meters. During stress period 2, each of the two wells shown on figure 14A withdraw water from the upper and lower aquifer at a rate of 72,000 cubic meters per day.

The initial steady-state stress period results in a maximum head of 143.0 meters in row 1, column 8. Steady-state hydraulic gradients slope down valley and toward the center of the valley to the constant-head cells in row 20, layers 1–4 (fig. 14). The steady-state head distribution is used to compute initial effective stress, preconsolidation stress, and geostatic stress for the transient part of the simulation. For the location of the well in row 9, column 10, layer 2, these stress values are 273.3, 288.3, and 509.5 meters, respectively.

Equivalent skeletal specific storage values were calculated from recompression and compression indices and the initial effective stress distribution. Computed values of elastic skeletal specific storage at row 9, column 10, were 2.03×10^{-5} , 8.58×10^{-6} , 7.33×10^{-6} , and 4.41×10^{-6} per meter for layers 1–4, respectively. Values of inelastic (virgin) skeletal specific storage for the same location were 2.03×10^{-4} , 8.58×10^{-5} , 7.33×10^{-5} , and 4.41×10^{-5} per meter for layers 1–4, respectively. These values are not used explicitly in further calculations by the CSUB package, but are provided to illustrate how effective stress influences the spatial distribution of specific storage.

Values of effective stress, preconsolidation stress, and geostatic stress at the bottom of the cell for the 60-year pumping and 60-year recovery periods are shown in figure 15 for row 9, column 10, layers 1 and 2. In both layers, preconsolidation stress is exceeded early in the simulation and tracks with increases in effective stress until recovery of water levels after the start of stress period 3 (year 60). Head change at this location is

similar in layers 1 and 2, and the shapes and magnitudes of change-of-effective- and preconsolidation-stress curves are nearly the same (figs. 15A, C). The curves, however, are at different head elevations because of the increase in magnitude of stress with depth. The shapes of curves representing geostatic stress in layers 1 and 2 (figs. 15B, D) are identical because all of the change results from movement of the water table in layer 1 (fig. 14B). Note how simulated effective stress and geostatic stress does not return to initial values 60 years after cessation of pumpage; approximately 2,000 years without pumping is required for simulated effective stress and geostatic stress at row 9, column 10, layers 1 and 2 to return initial values.

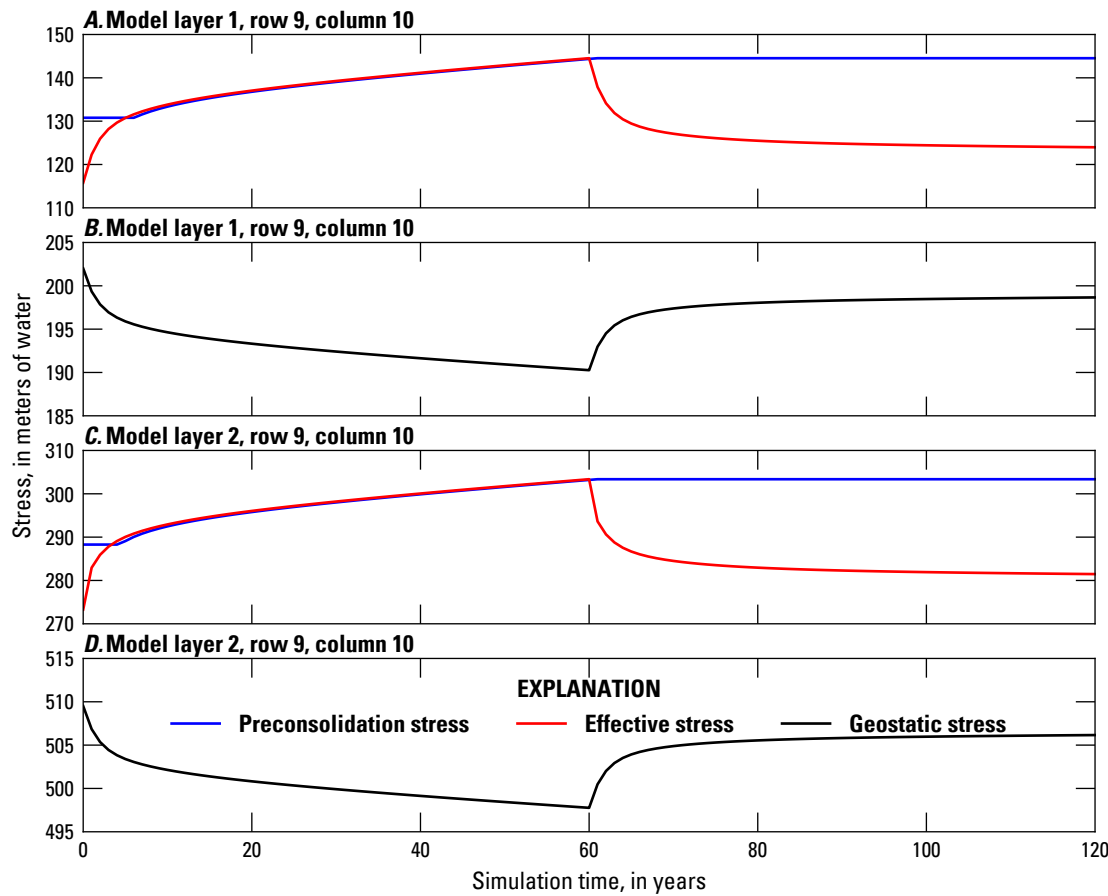


Figure 15. Graphs showing computed stresses for row 9, column 10 for the one-dimensional compaction in a three-dimensional flow field problem. A, Effective and preconsolidation stress in layer 1, B, geostatic stress in layer 1, C, effective and preconsolidation stress in layer 2, and D, geostatic stress in layer 2.

The computed vertical displacements for the tops of layers 1–4 resulting from fine- (interbed) and coarse-grained material compaction at the locations of the two pumping wells are shown in figure 16. The total compaction at the top of layer 1 represent the time series of land subsidence for the two locations (fig. 16E, F). Similarly, differences between displacement curves for adjacent layers are the time distributions of compaction in the each layer. At both locations, compaction is greatest in the layer in which pumping takes place. Coarse-grained compaction is small relative to inelastic compaction of fine-grained interbeds. Similar to stress results (fig. 15), elastic compaction of coarse-grained materials does not fully recover 60 years after cessation of

22 MODFLOW 6 CSUB Package Example Problems

pumpage.

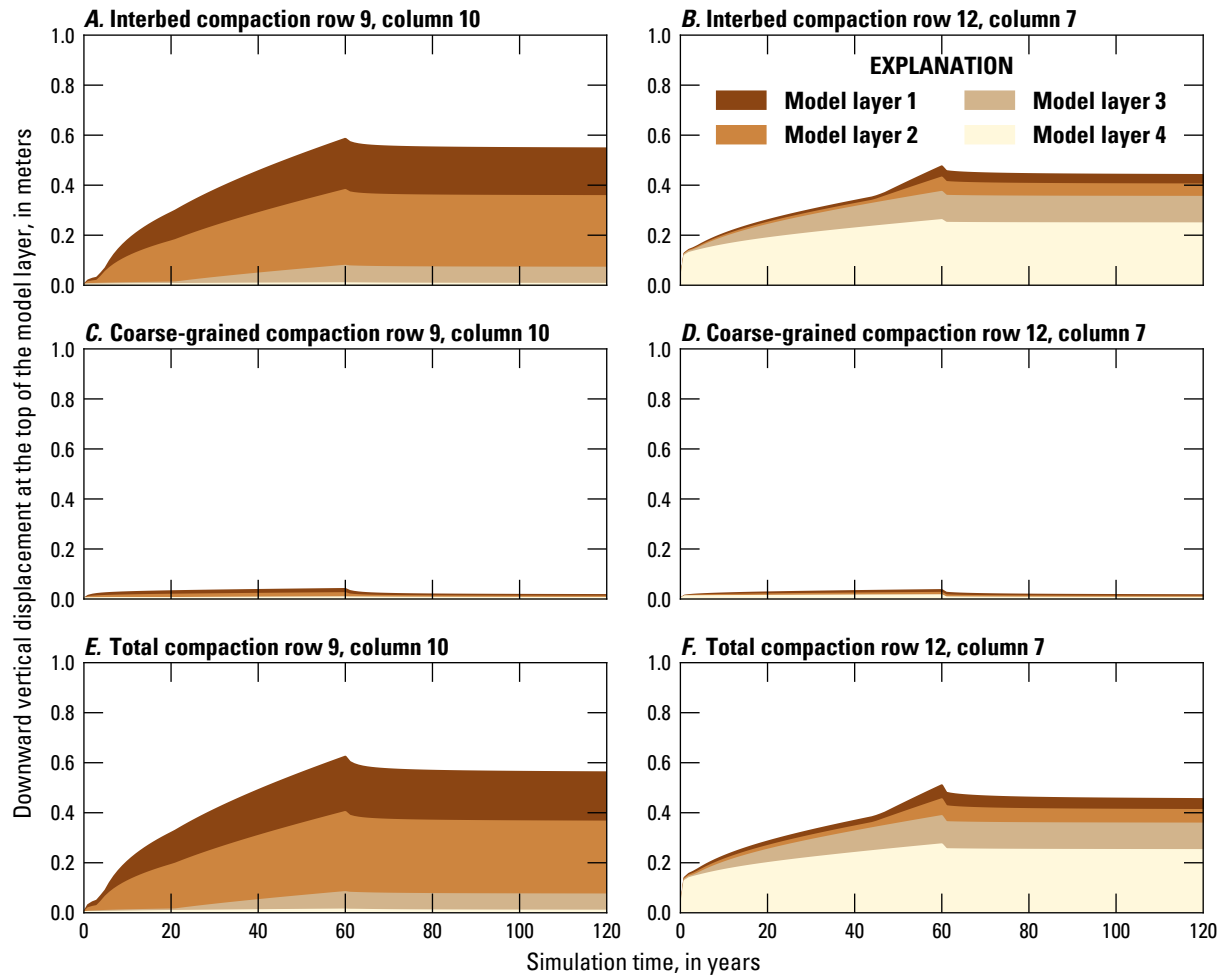


Figure 16. Graphs showing computed downward displacement for the tops of model layers 1–4 for the one-dimensional compaction in a three-dimensional flow field problem. *A*, interbed compaction at row 9, column 10, *B*, interbed compaction at row 12, column 7, *C*, coarse-grained material compaction at row 9, column 10, *D*, coarse-grained material compaction at row 12, column 7, *E*, total compaction at row 9, column 10, and *F*, total compaction at row 12, column 7.

At the end of the second stress period a total of 3,155,760,128 cubic meters of water was pumped from the water-table and confined aquifers. Water released from specific yield, elastic coarse-grained materials, elastic fine-grained materials, inelastic fine-grained materials, and water compressibility accounted for 96.31% (3,039,304,920 cubic meters) of groundwater pumpage; the remainder of groundwater pumpage came from reduction in the discharge to the eight constant-head cells. Individually specific yield, elastic coarse-grained materials, elastic fine-grained materials, inelastic fine-grained materials, and water compressibility accounted for 94.80%, 0.40%, 0.63%, 0.21%, and 0.27%, respectively, of total groundwater pumpage. For the cell containing well 1 (layer 2, row 9, column 10) elastic coarse-grained materials, elastic fine-grained materials, inelastic fine-grained materials, and water compressibility accounted for 5.18%, 3.81%, 87.68%, and 3.33%, respectively, of the total water released from storage (3,628.59 cubic meters) in response to groundwater pumpage. For the cell containing well 2 (layer 4, row 12, column 7) elastic coarse-grained materials, elastic fine-grained materials, inelastic fine-grained materials, and water compressibility accounted for 4.63%, 2.62%,

87.57%, and 5.18%, respectively, of the total water released from storage (3,147.01 cubic meters) in response to groundwater pumpage.

References Cited

- Burbey, T.J., 2001, Storage coefficient revisited: Is purely vertical strain a good assumption?: Groundwater, v. 39, no. 3, p. 458–464, accessed October 11, 2019, at <https://doi.org/10.1111/j.1745-6584.2001.tb02330.x>.
- Carlaw, H.S., and Jaeger, J.C., 1959, Conduction of heat in solids: Oxford: Clarendon Press, 1959, 2nd ed.
- Freeze, R.A., and Cherry, J.A., 1979, Groundwater: Englewood Cliffs, N.J., Prentice-Hall, 604 p.
- Hoffmann, Jörn, Leake, S.A., Galloway, D.L., and Wilson, A.M., 2003, MODFLOW-2000 Ground-Water Model—User Guide to the Subsidence and Aquifer-System Compaction (SUB) Package: U.S. Geological Survey Open-File Report 03–233, 44 p., accessed June 27, 2017, at <https://pubs.usgs.gov/of/2003/ofr03-233/>.
- Jacob, C.E., 1939, Fluctuations in artesian pressure produced by passing railroad-trains as shown in a well on Long Island, New York: Eos, Transactions American Geophysical Union, v. 20, no. 4, p. 666–674.
- Leake, S.A., and Galloway, D.L., 2007, MODFLOW Ground-water model—User guide to the Subsidence and Aquifer-System Compaction Package (SUB-WT) for Water-Table Aquifers: U.S. Geological Survey Techniques and Methods, book 6, chap. A23, 42 p., accessed June 27, 2017, at <https://pubs.er.usgs.gov/publication/tm6A23>.
- Riley, F.S., 1969, Analysis of borehole extensometer data from Central California: International Association of Scientific Hydrology Publication 89, v. 2, p. 423–431.
- Riley, F.S., 1998, Mechanics of aquifer systems—the scientific legacy of Joseph F. Poland, in Land subsidence case studies and current research: Proceedings of the Dr. Joseph F. Poland Symposium on Land Subsidence: Belmont, Calif., Star Publishing Co., Association of Engineering Geologists Special Publication, v. 8, p. 13–27.
- Sneed, Michelle, 2008, Aquifer-system compaction and land subsidence: data and simulations, the Holly site, Edwards Air Force Base, California: Sacramento, California State University, Master's Thesis, 40 p.
- Sneed, Michelle, and Galloway, D.L., 2000, Aquifer-system compaction and land subsidence: measurements, analyses, and simulations: the Holly Site, Edwards Air Force base, Antelope Valley, California: U.S. Geological Survey Water-Resources Investigations Report 2000–4015, 65 p., accessed July 9, 2019, at <https://pubs.er.usgs.gov/publication/wri20004015>.
- Welter, D.E., White, J.T., Hunt, R.J., and Doherty, J.E., 2015, Approaches in highly parameterized inversion—PEST++ Version 3, a Parameter ESTimation and uncertainty analysis software suite optimized for large environmental models: U.S. Geological Survey Techniques and Methods, book 7, section C12, 54 p., accessed April 18, 2019, at <https://doi.org/10.3133/tm7C12>.

Publishing support provided by the U.S. Geological Survey
MODFLOW 6 Development Team

For information concerning this publication, please contact:

Integrated Modeling and Prediction Division
U.S. Geological Survey
Mail Stop 411
12201 Sunrise Valley Drive
Reston, VA 20192
(703) 648-5001
<https://water.usgs.gov/ogw/>

